ISSN 1063-7729, Astronomy Reports, 2006, Vol. 50, No. 4, pp. 273–288. © Pleiades Publishing, Inc., 2006.
Original Russian Text © V.R. Amirkhanyan, 2006, published in Astronomicheskiĭ Zhurnal, 2006, Vol. 83, No. 4, pp. 310–326.

BVRI Observations of the Radio Source S5 0716+71

V. R. Amirkhanyan

Sternberg Astronomical Institute, Universitetskiĭ pr. 13, Moscow, 119992 Russia

Received April 6, 2005; in final form, September 7, 2005

Abstract—Photometric observations of the radio source S5 0716+714 were obtained in $BVRI$ filters from January 20, 1998 to January 9, 2001 with Zeiss-600 and Zeiss-1000 telescopes of the Special Astrophysical Observatory of the Russian Academy of Sciences. The light curves in all the bands are synchronous, providing evidence for the real variability of the object in timescales, from hundreds of days to 5–10 min. No time shift between events in the adjacent filters was detected. The variability spectrum at frequencies of 0.003–100 d^{-1} (3.5×10^{-8}–1.1×10^{-3} Hz) is close to that of a flicker noise. The optical spectral index α ($S \sim \nu^{\alpha}$) varies from -1.59 at the minimum to -1.13 at the maximum brightness. Measurements of linear polarization in BVR carried out on April 12–13, 2000 confirmed a high degree of polarization and rapid fluctuations of the polarization in a timescale of 15–30 min, whose amplitude decreases at red wavelengths. All the optical properties of the source, its compactness, the absence of spectral lines, the high degree of polarization, and very rapid fluctuations of the brightness, polarization, and spectral index, suggest a synchrotron origin for optical radiation. It may be that we are observing the radiation from a group of very compact bodies ($\sim 10^{-10}$ arcsec) at various stages of their evolution.

PACS numbers : 98.70.D
DOI: 10.1134/S1063772906040020

1. INTRODUCTION

The radio source S5 0716+71 was discovered in 1979 during the S5 survey [1]. Since then, it has been studied by numerous studies of radio to gamma-ray wavelengths. Comprehensive summaries of the properties of this object are given in [2–4]. It is classified as a BL Lac object, and is compact and variable, with a flat radio spectrum and a lineless optical spectrum. The source's brightness variability is extremely high and rapid even for this type of object.

2. PHOTOMETRY: OBSERVATIONS AND REDUCTION

We observed S5 0716+71 for three years, with the aim of distinguishing a periodic component in its light curve. Particular efforts were made to increase the accuracy of the measurements.

The observations were carried out with Zeiss-1000 and (mainly) Zeiss-600 telescopes of the Special Astrophysical Observatory (SAO), using the TAZIK automated photometer [5]. This photometer is equipped with Johnson–Cousins $BVRI$-filters, a shutter, an automatic guide mounted on an adjustable two-coordinate base, and a liquid-nitrogen-cooled CCD developed at the SAO, with 1050×1170 pixels 16×16 μm in size. In the case of the Zeiss-600 telescope, the pixel size is $0.45''$, and the field of view is $7.9' \times 8.8'$. Our software makes it possible to carry out long computer-controlled automated observations, providing homogeneous data that are free of human errors.

Depending on the state of the atmosphere and the brightness of the object, the exposure time was 120–180 s in the B filter, 90–120 s in the V filter, and 60–90 s in the R and I filters. Since we were interested in detecting small-scale variability with a maximum time resolution, the observations on each observing night were carried out continuously. If observations were made in all four filters, the time between exposures in the same filter was 9–15 min. We sometimes used only two filters, usually V and R, thus shortening this time to 2–5 min.

The dark and flat fields needed for CCD-image reduction were obtained for each observing night. Our experience indicated that the best flat field is provided by pixel-to-pixel median averaging of 10 to 20 images obtained during a single night in a given filter, with the same exposure but for different areas of sky. Images of the same field may be used if the telescope is shifted by $15''$–$20''$ between exposures. When we were unable to collect a sufficient number of images during a night, we averaged five morning or evening twilight exposures. To ensure similar background levels in flat fields obtained under conditions of rapidly varying sky brightness, we used the small guide CCD as an exposure meter to determine the exposure for the main CCD. Twilight exposures yield poorer flat

Table 1. $BVRI$ photometry

B								
JD−2450000	m_B	σ	JD−2450000	m_B	σ	JD−2450000	m_B	σ
1006.3695	14.63	0.013	1487.5771	15.32	0.023	1512.5765	15.28	0.033
1006.3785	14.64	0.018	1487.5890	15.30	0.02	1512.5876	15.34	0.03
1006.3870	14.64	0.018	1487.6008	15.29	0.023	1512.5980	15.56	0.027
1010.3501	14.84	0.025	1487.6174	15.27	0.02	1512.6084	15.39	0.025
1010.3682	14.84	0.025	1487.6285	15.29	0.02	1512.6313	15.52	0.033
1162.3717	14.55	0.027	1489.5745	14.96	0.018	1512.6411	15.35	0.02
1162.3932	14.50	0.02	1489.5862	14.96	0.018	1512.6515	15.49	0.038
1162.4147	14.58	0.02	1489.5980	15.00	0.02	1512.6633	15.55	0.023
1162.4369	14.38	0.02	1489.6099	14.96	0.023	1512.6737	15.49	0.02
1162.4585	14.54	0.018	1489.6251	14.94	0.02	1572.3369	14.53	0.025
1162.4792	14.68	0.02	1489.6370	14.94	0.02	1572.3487	14.50	0.02
1162.5015	14.73	0.02	1489.6487	14.92	0.015	1572.3606	14.53	0.015
1162.5231	14.51	0.027	1489.6605	14.95	0.015	1572.3730	14.54	0.018
1162.5453	14.53	0.023	1493.5453	15.02	0.018	1572.3862	14.51	0.018
1162.5668	14.56	0.018	1493.5688	15.04	0.02	1572.3981	14.53	0.015
1169.4911	14.87	0.018	1493.5807	15.06	0.038	1572.4820	14.63	0.018
1169.5120	14.86	0.013	1493.5959	15.05	0.02	1572.4939	14.61	0.015
1169.5327	14.92	0.025	1493.6078	15.08	0.027	1572.5063	14.60	0.018
1169.5536	14.84	0.018	1493.6195	15.02	0.018	1572.5210	14.62	0.02
1169.5779	14.81	0.015	1493.6313	15.08	0.018	1572.5327	14.65	0.02
1198.3028	14.78	0.023	1493.6445	15.08	0.015	1572.5453	14.65	0.02
1198.3293	14.83	0.018	1494.5487	14.97	0.02	1572.5688	14.67	0.018
1198.3522	14.82	0.033	1494.5598	14.96	0.023	1572.5925	14.71	0.018
1198.3785	14.87	0.02	1494.5716	14.82	0.033	1572.6057	14.71	0.025
1198.3939	14.83	0.023	1494.5946	14.99	0.027	1572.6182	14.72	0.02
1198.5050	14.8	0.018	1494.6063	14.99	0.027	1572.6300	14.76	0.02
1198.5668	14.78	0.018	1494.6182	15.04	0.018	1572.6453	14.83	0.023
1198.5939	14.84	0.02	1494.6418	15.01	0.02	1572.6571	14.79	0.02
1486.5494	15.16	0.018	1512.4877	15.34	0.023	1605.3293	14.73	0.02
1486.5613	15.16	0.018	1512.4988	15.32	0.018	1605.3758	14.78	0.023
1486.5730	15.16	0.023	1512.5084	15.38	0.025	1605.3890	14.74	0.018
1486.5848	15.16	0.02	1512.5195	15.36	0.018	1605.4043	14.75	0.018
1486.6050	15.18	0.023	1512.5293	15.36	0.018	1605.4167	14.74	0.02
1486.6168	15.15	0.018	1512.5397	15.38	0.025	1605.4383	14.80	0.02
1486.6396	15.19	0.025	1512.5557	15.34	0.027	1605.4466	14.76	0.025
1486.6508	15.20	0.023	1512.5660	15.33	0.023	1608.3293	14.82	0.018

Table 1. (Contd.)

B								
JD−2450000	m_B	σ	JD−2450000	m_B	σ	JD−2450000	m_B	σ
1608.3362	14.86	0.027	1635.2661	15.38	0.027	1855.5370	13.80	0.023
1608.3431	14.85	0.02	1635.2737	15.35	0.03	1855.5445	13.77	0.02
1608.3522	14.82	0.023	1635.2897	15.29	0.02	1855.5521	14.56	0.025
1608.5737	14.92	0.07	1635.2974	15.34	0.02	1855.5604	13.71	0.025
1608.5828	14.93	0.033	1635.3049	15.36	0.03	1855.5682	13.78	0.038
1611.3550	14.69	0.02	1635.3196	15.29	0.023	1855.5917	13.72	0.03
1611.3627	14.68	0.027	1636.2383	15.25	0.038	1855.5995	13.79	0.018
1611.3702	14.70	0.018	1636.246	15.24	0.023	1855.6070	13.69	0.018
1611.3779	14.74	0.013	1636.2535	15.27	0.02	1855.6146	13.75	0.025
1611.3870	14.82	0.033	1636.262	15.27	0.03	1855.6224	13.65	0.02
1611.4043	14.71	0.02	1636.2695	15.26	0.018	1855.6300	13.78	0.02
1611.4120	14.71	0.018	1636.4237	15.31	0.03	1855.6376	13.73	0.018
1611.4195	14.74	0.018	1636.4342	15.29	0.018	1868.5113	13.86	0.018
1615.2341	14.83	0.018	1636.4515	15.26	0.018	1868.5189	13.89	0.02
1615.2460	14.73	0.038	1646.2751	14.62	0.018	1868.5272	13.80	0.018
1615.2535	14.89	0.015	1646.2821	14.6	0.015	1868.5348	13.78	0.015
1615.2682	14.90	0.015	1646.2897	14.63	0.018	1868.5509	13.76	0.023
1618.3570	14.93	0.018	1646.2974	14.63	0.015	1868.5592	13.76	0.018
1618.3647	14.91	0.018	1646.3064	14.63	0.018	1868.5668	13.88	0.023
1618.3723	14.95	0.02	1646.3133	14.6	0.023	1868.5870	13.81	0.015
1618.3800	14.92	0.02	1646.3209	14.66	0.018	1868.5953	13.91	0.018
1618.3883	14.89	0.015	1646.3286	14.62	0.02	1868.6029	13.85	0.018
1618.3960	14.91	0.023	1850.5306	14.21	0.033	1868.6105	13.90	0.018
1618.4050	14.96	0.02	1850.5431	14.23	0.02	1868.6188	13.89	0.02
1618.4126	14.94	0.02	1850.5528	14.23	0.025	1868.6266	13.85	0.018
1618.4203	14.95	0.018	1850.5619	14.24	0.015	1868.6349	13.87	0.02
1619.2563	15.01	0.018	1850.5716	14.17	0.018	1868.6424	13.82	0.018
1619.4258	15.07	0.02	1850.5814	14.2	0.018	1904.3751	14.27	0.015
1619.4327	15.04	0.018	1850.5939	14.18	0.015	1904.4008	14.24	0.018
1619.4390	14.98	0.023	1850.6168	14.22	0.03	1904.4120	14.25	0.018
1620.2473	15.32	0.02	1850.6266	14.25	0.025	1904.4230	14.17	0.023
1620.2599	15.34	0.02	1850.6363	14.21	0.015	1904.4342	14.26	0.02
1620.2695	15.37	0.023	1852.6161	13.76	0.033	1904.4530	14.27	0.013
1620.2786	15.31	0.03	1852.6390	13.72	0.02	1904.4640	14.24	0.02
1620.2876	15.33	0.023	1852.6473	13.64	0.018	1904.4752	14.23	0.018
1620.2974	15.49	0.023	1852.6549	13.74	0.027	1904.4869	14.24	0.018

Table 1. (Contd.)

B								
JD−2450000	m_B	σ	JD−2450000	m_B	σ	JD−2450000	m_B	σ
1904.4979	14.26	0.018	1904.5973	14.27	0.018	1918.4354	13.98	0.018
1904.5099	14.26	0.018	1904.6085	14.27	0.018	1918.4432	14.00	0.02
1904.5314	14.20	0.015	1904.6202	14.24	0.018	1918.4508	13.95	0.02
1904.5426	14.22	0.018	1904.6315	14.23	0.03	1918.4662	13.96	0.018
1904.5543	14.17	0.015	1904.6432	14.22	0.018	1918.4737	13.99	0.018
1904.5660	14.27	0.018	1918.4203	14.00	0.035	1918.4813	14.01	0.015
1904.5780	14.28	0.013	1918.4278	13.99	0.018	1918.4889	14.01	0.018
V								
JD−2450000	m_V	σ	JD−2450000	m_V	σ	JD−2450000	m_V	σ
1006.3653	14.2	0.015	1142.5174	13.50	0.015	1487.5744	14.81	0.018
1006.3743	14.19	0.013	1162.3674	14.10	0.013	1487.5972	14.81	0.018
1006.3828	14.17	0.015	1162.3890	14.11	0.02	1487.6140	14.79	0.018
1010.3528	14.4	0.027	1162.4112	14.12	0.013	1487.6258	14.76	0.015
1010.3709	14.41	0.018	1162.4327	14.10	0.013	1489.5709	14.53	0.015
1139.4112	13.72	0.01	1162.4549	14.18	0.013	1489.5827	14.53	0.01
1139.4236	13.49	0.013	1162.4750	14.15	0.018	1489.6063	14.55	0.018
1139.4299	13.52	0.013	1162.4973	14.18	0.013	1489.6223	14.54	0.018
1139.4660	13.61	0.008	1162.5189	14.14	0.015	1489.6341	14.54	0.023
1139.4730	13.62	0.015	1162.5411	14.15	0.015	1489.6459	14.49	0.015
1139.4973	13.65	0.015	1198.2980	14.34	0.013	1489.6577	14.52	0.02
1139.5029	13.67	0.015	1198.3250	14.38	0.015	1493.5417	14.59	0.013
1139.5417	13.73	0.015	1198.3472	14.17	0.015	1493.5535	14.61	0.013
1139.5535	13.74	0.013	1198.3737	14.33	0.015	1493.5654	14.65	0.013
1140.4265	13.39	0.023	1198.3890	14.33	0.015	1493.5771	14.66	0.02
1140.4327	13.37	0.018	1198.5001	14.31	0.015	1493.5925	14.66	0.015
1140.4591	13.39	0.018	1198.5626	14.38	0.015	1493.6042	14.65	0.018
1140.4660	13.37	0.013	1198.5889	14.40	0.03	1493.6160	14.66	0.015
1140.4876	13.36	0.013	1486.5458	14.69	0.01	1493.6279	14.67	0.02
1140.4918	13.38	0.015	1486.5577	14.69	0.018	1493.6411	14.67	0.025
1142.4368	13.72	0.018	1486.5695	14.72	0.015	1494.5452	14.54	0.01
1142.4424	13.65	0.013	1486.5814	14.72	0.013	1494.5570	14.55	0.015
1142.4591	13.71	0.013	1486.6021	14.73	0.018	1494.5682	14.57	0.023
1142.4654	13.70	0.01	1486.6140	14.7	0.013	1494.5917	14.52	0.013
1142.4876	13.63	0.01	1486.6424	14.73	0.02	1494.6036	14.59	0.018
1142.4918	13.60	0.013	1486.6529	14.79	0.023	1494.6147	14.56	0.02
1142.5140	13.46	0.013	1487.5618	14.84	0.013	1494.6382	14.65	0.013

Table 1. (Contd.)

V								
JD−2450000	m_V	σ	JD−2450000	m_V	σ	JD−2450000	m_V	σ
1572.3334	14.03	0.035	1611.3605	14.23	0.013	1635.2952	14.84	0.023
1572.3452	14.02	0.015	1611.3751	14.30	0.01	1635.3022	14.83	0.015
1572.3577	14.08	0.013	1611.3828	14.27	0.013	1635.3098	14.94	0.025
1572.3695	14.09	0.015	1611.3939	14.30	0.015	1636.2361	14.77	0.03
1572.3828	14.03	0.015	1611.4014	14.28	0.015	1636.2508	14.73	0.02
1572.3952	14.04	0.01	1611.4091	14.26	0.015	1636.2584	14.72	0.013
1572.4786	14.08	0.015	1611.4167	14.30	0.013	1636.2668	14.71	0.02
1572.4910	14.13	0.015	1615.2313	14.38	0.015	1636.4195	14.75	0.013
1572.5029	14.15	0.015	1615.2431	14.38	0.033	1636.4299	14.76	0.015
1572.5174	14.17	0.023	1615.2508	14.41	0.013	1636.4473	14.76	0.013
1572.5292	14.17	0.013	1615.2584	14.43	0.01	1636.4695	14.82	0.015
1572.5417	14.15	0.015	1615.2661	14.41	0.015	1646.2723	14.14	0.015
1572.5654	14.18	0.015	1618.3549	14.44	0.013	1646.2800	14.14	0.013
1572.5771	14.22	0.018	1618.3619	14.45	0.023	1646.2875	14.17	0.018
1572.5897	14.24	0.015	1618.3695	14.46	0.018	1646.2945	14.15	0.015
1572.6021	14.25	0.02	1618.3771	14.48	0.018	1646.3022	14.14	0.015
1572.6147	14.25	0.018	1618.3862	14.44	0.013	1646.3112	14.17	0.015
1572.6264	14.27	0.025	1618.3939	14.44	0.015	1646.3188	14.16	0.015
1572.6418	14.25	0.018	1618.4022	14.45	0.015	1646.3257	14.11	0.013
1605.2800	14.29	0.015	1618.4097	14.47	0.023	1849.6209	13.32	0.013
1605.3257	14.32	0.018	1618.4174	14.46	0.015	1849.6307	13.26	0.018
1605.3397	14.30	0.015	1619.2535	14.56	0.015	1849.6500	13.32	0.055
1605.3521	14.29	0.018	1619.4236	14.54	0.015	1850.5494	13.77	0.013
1605.3716	14.24	0.015	1619.4306	14.53	0.015	1850.5591	13.76	0.015
1605.3848	14.29	0.018	1619.4368	14.51	0.013	1850.5682	13.74	0.013
1605.4001	14.24	0.015	1620.2445	14.80	0.018	1850.5779	13.69	0.01
1605.4133	14.29	0.015	1620.2563	14.80	0.025	1850.5904	13.70	0.015
1605.4355	14.31	0.015	1620.2661	14.85	0.015	1850.6002	13.74	0.025
1605.4438	14.25	0.015	1620.2751	14.80	0.018	1850.6138	13.74	0.015
1608.3271	14.35	0.013	1620.2847	14.87	0.03	1850.6229	13.76	0.018
1608.3341	14.33	0.018	1620.2938	14.86	0.02	1850.6326	13.70	0.018
1608.3410	14.34	0.02	1635.2563	14.80	0.02	1852.5987	13.28	0.015
1608.3500	14.36	0.013	1635.2632	14.84	0.02	1852.6138	13.31	0.023
1608.5716	14.48	0.018	1635.2709	14.85	0.018	1852.6292	13.27	0.015
1608.5806	14.46	0.02	1635.2785	14.84	0.023	1852.6446	13.25	0.033
1611.3528	14.23	0.013	1635.2862	14.83	0.015	1855.5181	13.35	0.018

Table 1. (Contd.)

V								
JD−2450000	m_V	σ	JD−2450000	m_V	σ	JD−2450000	m_V	σ
1855.5347	13.37	0.023	1868.5924	13.33	0.018	1904.5389	13.81	0.013
1855.5425	13.38	0.013	1868.6007	13.42	0.018	1904.5618	13.85	0.007
1855.5501	13.26	0.015	1868.6085	13.41	0.013	1904.5731	13.84	0.013
1855.5577	13.35	0.018	1868.6160	13.39	0.018	1904.5931	13.88	0.013
1855.5653	13.32	0.023	1868.6243	13.32	0.015	1904.6050	13.85	0.013
1855.5731	13.31	0.018	1868.6319	13.47	0.025	1904.6160	13.83	0.01
1855.5889	13.39	0.02	1868.6397	13.38	0.015	1904.6278	13.79	0.007
1855.5965	13.34	0.018	1904.3709	13.86	0.015	1904.6390	13.74	0.015
1855.6043	13.32	0.015	1904.3863	13.82	0.01	1918.4175	13.59	0.015
1855.6119	13.32	0.018	1904.3973	13.82	0.01	1918.4251	13.53	0.023
1855.6202	13.23	0.02	1904.4085	13.81	0.013	1918.4327	13.60	0.023
1855.6278	13.31	0.018	1904.4195	13.81	0.013	1918.4403	13.55	0.023
1868.5084	13.38	0.01	1904.4307	13.79	0.013	1918.4481	13.56	0.015
1868.5167	13.37	0.015	1904.4488	13.84	0.013	1918.4556	13.54	0.013
1868.5245	13.37	0.015	1904.4598	13.84	0.015	1918.4632	13.56	0.018
1868.5328	13.34	0.018	1904.4710	13.81	0.015	1918.4710	13.57	0.023
1868.5479	13.41	0.02	1904.4827	13.78	0.013	1918.4786	13.57	0.02
1868.5562	13.39	0.015	1904.4937	13.81	0.013	1918.4861	13.58	0.018
1868.5648	13.41	0.015	1904.5057	13.80	0.013			
1868.5848	13.43	0.015	1904.5272	13.83	0.01			
R								
JD−2450000	m_R	σ	JD−2450000	m_R	σ	JD−2450000	m_R	σ
833.5014	13.5	0.018	1139.4090	13.31	0.013	1142.4570	13.29	0.013
837.3104	13.41	0.015	1139.4264	13.23	0.018	1142.4632	13.29	0.015
841.3465	13.43	0.073	1139.4632	13.19	0.015	1142.4861	13.21	0.018
841.3583	13.41	0.01	1139.4702	13.19	0.013	1142.4896	13.19	0.013
841.5465	13.41	0.043	1139.4945	13.25	0.013	1142.5118	13.06	0.018
905.2722	13.33	0.01	1139.5396	13.29	0.018	1142.5153	13.09	0.018
905.2743	13.35	0.015	1139.5507	13.33	0.02	1162.3632	13.67	0.015
906.3320	13.53	0.018	1140.4236	12.98	0.018	1162.3861	13.64	0.015
906.3333	13.52	0.015	1140.4299	12.94	0.013	1162.4077	13.69	0.013
1006.3625	13.81	0.015	1140.4549	12.95	0.018	1162.4292	13.72	0.02
1006.3722	13.76	0.013	1140.4847	12.99	0.013	1162.4514	13.72	0.013
1006.3806	13.74	0.015	1140.4896	12.98	0.02	1162.4715	13.71	0.015
1010.3465	13.95	0.018	1142.4340	13.31	0.033	1162.4938	13.72	0.01
1010.3646	14.06	0.025	1142.4396	13.26	0.015	1162.5153	13.74	0.01

Table 1. (Contd.)

R								
JD−2450000	m_R	σ	JD−2450000	m_R	σ	JD−2450000	m_R	σ
1162.5375	13.67	0.015	1489.5799	14.09	0.015	1572.5389	13.71	0.015
1162.5590	13.73	0.013	1489.5917	14.09	0.018	1572.5625	13.75	0.023
1167.3472	14.19	0.015	1489.6035	14.12	0.02	1572.5750	13.75	0.015
1167.3688	14.22	0.015	1489.6195	14.10	0.015	1572.5868	13.73	0.015
1167.3896	14.25	0.015	1489.6313	14.08	0.023	1572.6118	13.75	0.013
1167.3993	14.20	0.01	1489.6431	14.09	0.02	1572.6243	13.77	0.02
1167.4202	14.19	0.013	1489.6549	14.08	0.018	1572.6514	13.78	0.015
1167.4417	14.18	0.013	1493.5389	14.18	0.018	1605.2771	13.82	0.02
1167.4632	14.18	0.015	1493.5507	14.23	0.025	1605.3104	13.86	0.023
1167.4840	14.21	0.015	1493.5625	14.20	0.013	1605.3361	13.87	0.015
1167.4938	14.24	0.013	1493.5743	14.21	0.015	1605.3486	13.81	0.018
1167.5146	14.19	0.01	1493.5903	14.24	0.015	1605.3688	13.83	0.013
1167.5354	14.21	0.013	1493.6021	14.25	0.015	1605.3813	13.82	0.02
1167.5563	14.21	0.013	1493.6139	14.20	0.018	1605.3945	13.83	0.015
1169.4833	13.99	0.015	1493.6257	14.25	0.025	1605.4097	13.86	0.015
1169.5042	13.98	0.015	1493.6389	14.30	0.057	1605.4333	13.85	0.018
1169.5250	13.98	0.015	1494.5660	14.15	0.018	1605.4417	13.83	0.013
1169.5465	13.98	0.01	1494.5778	14.14	0.018	1608.3250	13.91	0.015
1169.5702	13.95	0.013	1494.5889	14.12	0.015	1608.3320	13.90	0.015
1198.2938	13.80	0.013	1494.6007	14.17	0.015	1608.3396	13.87	0.013
1198.3208	13.78	0.033	1494.6354	14.18	0.015	1608.3479	13.87	0.018
1198.3431	13.97	0.038	1512.4827	14.42	0.02	1608.5785	14.12	0.04
1198.3847	13.98	0.018	1512.5827	14.40	0.013	1611.3507	13.83	0.018
1198.4958	13.90	0.02	1512.6035	14.31	0.02	1611.3583	13.78	0.015
1198.5583	13.96	0.013	1512.6257	14.37	0.023	1611.3660	13.79	0.013
1198.5847	13.93	0.015	1512.6368	14.39	0.013	1611.3736	13.80	0.018
1486.5431	14.24	0.015	1512.6472	14.20	0.018	1611.3813	13.82	0.02
1486.5549	14.28	0.015	1512.6590	14.24	0.023	1611.3924	13.83	0.013
1486.5667	14.25	0.018	1512.6688	14.55	0.027	1611.4000	13.80	0.015
1486.5785	14.30	0.023	1512.6792	14.51	0.027	1611.4070	13.80	0.018
1486.5993	14.27	0.015	1572.3306	13.58	0.01	1611.4146	13.90	0.018
1486.6111	14.29	0.02	1572.3431	13.59	0.015	1615.2292	13.87	0.013
1486.6445	14.28	0.015	1572.3549	13.57	0.015	1615.2417	13.94	0.018
1486.6549	14.27	0.018	1572.3674	13.59	0.013	1615.2493	13.93	0.013
1487.5597	14.39	0.015	1572.3792	13.59	0.013	1615.2570	13.97	0.015
1487.5715	14.37	0.015	1572.3924	13.60	0.013	1615.2639	13.91	0.013
1487.5833	14.34	0.015	1572.4757	13.63	0.015	1618.3521	13.99	0.018
1487.5952	14.31	0.013	1572.4882	13.68	0.015	1618.3604	14.01	0.02
1487.6111	14.30	0.013	1572.5000	13.67	0.015	1618.3681	14.02	0.018
1489.5681	14.10	0.015	1572.5271	13.67	0.015	1618.3757	13.99	0.018

Table 1. (Contd.)

R								
JD−2450000	m_R	σ	JD−2450000	m_R	σ	JD−2450000	m_R	σ
1618.3840	13.97	0.018	1849.6188	12.86	0.02	1868.5625	12.92	0.015
1618.3993	13.97	0.018	1849.6278	12.86	0.013	1868.5827	12.98	0.015
1618.4083	13.99	0.018	1849.6375	12.83	0.015	1868.5910	12.96	0.013
1618.4153	13.99	0.015	1849.6472	12.84	0.015	1868.5986	12.96	0.018
1619.2521	14.09	0.015	1849.6570	12.86	0.018	1868.6063	12.97	0.015
1619.4222	14.10	0.018	1850.5243	13.23	0.013	1868.6222	12.94	0.015
1619.4285	14.07	0.018	1850.5375	13.27	0.015	1868.6299	12.97	0.015
1619.4354	14.04	0.015	1850.5472	13.24	0.015	1868.6382	12.97	0.015
1620.2417	14.32	0.023	1850.5570	13.28	0.015	1904.3681	13.43	0.015
1620.2542	14.31	0.015	1850.5660	13.27	0.023	1904.3833	13.42	0.013
1620.2639	14.26	0.02	1850.5979	13.23	0.02	1904.3945	13.41	0.013
1620.2729	14.36	0.018	1850.6118	13.28	0.015	1904.4056	13.38	0.015
1620.2827	14.34	0.02	1850.6306	13.29	0.02	1904.4167	13.40	0.018
1620.2917	14.40	0.025	1852.5965	12.88	0.013	1904.4278	13.37	0.013
1635.2542	14.31	0.015	1852.6042	12.86	0.018	1904.4458	13.43	0.013
1635.2695	14.45	0.027	1852.6118	12.88	0.025	1904.4570	13.41	0.013
1635.2764	14.41	0.033	1852.6271	12.86	0.02	1904.4688	13.40	0.013
1635.2840	14.36	0.023	1852.6347	12.88	0.02	1904.4799	13.40	0.015
1635.2931	14.37	0.018	1852.6431	12.76	0.033	1904.4917	13.40	0.015
1635.3007	14.37	0.023	1852.6507	12.86	0.015	1904.5028	13.41	0.015
1635.3083	14.42	0.025	1855.5160	12.95	0.015	1904.5250	13.40	0.013
1636.2340	14.28	0.023	1855.5250	12.91	0.015	1904.5361	13.38	0.013
1636.2417	14.28	0.025	1855.5327	12.98	0.018	1904.5479	13.38	0.013
1636.2493	14.26	0.023	1855.5403	12.95	0.015	1904.5590	13.40	0.013
1636.2563	14.3	0.023	1855.5556	12.94	0.015	1904.5708	13.41	0.008
1636.2653	14.24	0.018	1855.5715	12.91	0.01	1904.5903	13.44	0.015
1636.4167	14.29	0.023	1855.5952	12.94	0.015	1904.6021	13.41	0.01
1636.4278	14.28	0.015	1855.6028	12.91	0.018	1904.6132	13.41	0.015
1636.4396	14.27	0.013	1855.6104	12.92	0.015	1904.6250	13.40	0.01
1636.4556	14.31	0.018	1855.6181	12.88	0.018	1904.6368	13.33	0.015
1636.4667	14.34	0.02	1855.6257	12.88	0.018	1918.4160	13.13	0.025
1646.2702	13.70	0.013	1855.6333	12.91	0.018	1918.4313	13.18	0.018
1646.2854	13.69	0.015	1868.5063	12.97	0.015	1918.4389	13.16	0.013
1646.2931	13.68	0.015	1868.5146	12.91	0.015	1918.4465	13.18	0.02
1646.3007	13.66	0.013	1868.5222	12.93	0.018	1918.4542	13.16	0.018
1646.3090	13.69	0.015	1868.5306	12.93	0.013	1918.4695	13.10	0.02
1646.3167	13.66	0.018	1868.5382	12.96	0.015	1918.4771	13.13	0.015
1646.3243	13.69	0.015	1868.5465	12.93	0.013	1918.4847	13.13	0.015
1646.3320	13.72	0.015	1868.5542	12.94	0.013			

Table 1. (Contd.)

I								
JD−2450000	m_I	σ	JD−2450000	m_I	σ	JD−2450000	m_I	σ
1512.4896	13.86	0.018	1608.3305	13.35	0.018	1635.2750	13.85	0.023
1512.5000	13.84	0.023	1608.3381	13.32	0.018	1635.2826	13.82	0.02
1512.5104	13.87	0.02	1608.3451	13.32	0.018	1635.2916	13.81	0.02
1512.5209	13.82	0.02	1608.3535	13.35	0.015	1635.2993	13.77	0.02
1512.5888	13.84	0.015	1608.5757	13.44	0.02	1635.3063	13.83	0.02
1512.5993	13.86	0.02	1608.5840	13.38	0.027	1635.3138	13.84	0.018
1512.6097	13.88	0.023	1611.3569	13.27	0.018	1635.3222	13.81	0.018
1512.6327	13.84	0.025	1611.3646	13.30	0.015	1636.2402	13.68	0.018
1512.6430	13.88	0.02	1611.3722	13.28	0.015	1636.2479	13.68	0.023
1512.6534	13.90	0.023	1611.3799	13.29	0.018	1636.2549	13.69	0.02
1512.6653	13.89	0.04	1611.3910	13.28	0.015	1636.2639	13.69	0.023
1512.6756	14.15	0.018	1611.3979	13.30	0.02	1636.2709	13.69	0.02
1572.3388	13.04	0.018	1611.4055	13.27	0.015	1636.4256	13.73	0.018
1572.3507	13.03	0.018	1611.4132	13.29	0.018	1636.4375	13.74	0.018
1572.3625	13.05	0.015	1611.4208	13.27	0.018	1636.4535	13.73	0.018
1572.3750	13.05	0.018	1615.2361	13.36	0.023	1636.4653	13.77	0.023
1572.3882	13.04	0.015	1615.2381	13.38	0.018	1636.4757	13.75	0.018
1572.4000	13.13	0.03	1615.2479	13.37	0.018	1646.2763	13.16	0.018
1572.4840	13.11	0.023	1615.2549	13.36	0.015	1646.2840	13.16	0.018
1572.4958	13.11	0.018	1615.2624	13.37	0.015	1646.2916	13.14	0.015
1572.5083	13.13	0.02	1615.2694	13.36	0.018	1646.2986	13.16	0.02
1572.5229	13.13	0.015	1618.3590	13.44	0.015	1646.3076	13.15	0.018
1572.5346	13.12	0.015	1618.3667	13.42	0.018	1646.3153	13.15	0.015
1572.5472	13.17	0.023	1618.3742	13.45	0.02	1646.3229	13.15	0.018
1572.5708	13.17	0.015	1618.3812	13.40	0.015	1646.3305	13.18	0.018
1572.5826	13.14	0.023	1618.3902	13.39	0.018	1849.6355	12.36	0.02
1572.5945	13.21	0.02	1618.3979	13.44	0.02	1849.6450	12.36	0.023
1572.6076	13.20	0.023	1618.4062	13.48	0.023	1850.5339	12.74	0.02
1572.6201	13.25	0.015	1618.4139	13.42	0.02	1850.5549	12.74	0.018
1572.6319	13.22	0.015	1618.4215	13.44	0.018	1850.5639	12.76	0.02
1572.6472	13.26	0.018	1619.2577	13.54	0.018	1850.5737	12.73	0.023
1572.6590	13.26	0.02	1619.4271	13.51	0.018	1850.5832	12.70	0.015
1605.3334	13.30	0.023	1619.4341	13.49	0.018	1850.5964	12.73	0.02
1605.3465	13.27	0.02	1619.4403	13.48	0.018	1850.6186	12.73	0.025
1605.3597	13.26	0.02	1620.2492	13.71	0.023	1850.6284	12.67	0.018
1605.3917	13.31	0.018	1620.2618	13.79	0.023	1850.6382	12.76	0.023
1605.4070	13.34	0.018	1620.2715	13.76	0.023	1852.6028	12.39	0.045
1605.4201	13.32	0.013	1620.2805	13.78	0.02	1852.6103	12.41	0.023
1605.4396	13.29	0.018	1620.2895	13.82	0.023	1852.6181	12.40	0.023
1605.4479	13.32	0.018	1635.2604	13.79	0.02	1852.6333	12.35	0.02

Table 1. (Contd.)

I								
JD−2450000	m_I	σ	JD−2450000	m_I	σ	JD−2450000	m_I	σ
1852.6416	12.36	0.015	1868.5603	12.41	0.018	1904.5124	12.90	0.015
1852.6494	12.32	0.02	1868.5688	12.43	0.015	1904.5339	12.91	0.015
1852.6570	12.34	0.02	1868.5888	12.43	0.02	1904.5451	12.92	0.018
1855.5466	12.47	0.02	1868.5964	12.41	0.018	1904.5569	12.90	0.018
1855.5542	12.38	0.015	1868.6050	12.43	0.018	1904.5681	12.90	0.015
1855.5617	12.56	0.035	1868.6125	12.31	0.025	1904.5813	12.92	0.018
1855.5693	12.32	0.023	1868.6201	12.43	0.015	1904.5993	12.91	0.015
1855.5779	12.40	0.023	1868.6284	12.40	0.018	1904.6111	12.93	0.018
1855.5930	12.46	0.018	1868.6362	12.43	0.015	1904.6228	12.89	0.018
1855.6006	12.45	0.025	1868.6438	12.47	0.018	1904.6340	12.89	0.015
1855.6084	12.39	0.018	1904.3772	12.91	0.015	1904.6450	12.87	0.015
1855.6159	12.42	0.02	1904.3923	12.92	0.02	1918.4221	12.75	0.025
1855.6242	12.41	0.018	1904.4035	12.90	0.015	1918.4299	12.68	0.018
1855.6318	12.41	0.018	1904.4145	12.90	0.015	1918.4375	12.68	0.018
1855.6396	12.40	0.02	1904.4258	12.94	0.03	1918.4529	12.63	0.015
1868.5132	12.39	0.015	1904.4367	12.92	0.015	1918.4604	12.65	0.02
1868.5207	12.42	0.018	1904.4548	12.90	0.015	1918.4680	12.65	0.02
1868.5285	12.44	0.02	1904.4660	12.92	0.018	1918.4756	12.65	0.02
1868.5368	12.44	0.018	1904.4778	12.90	0.018	1918.4834	12.66	0.015
1868.5444	12.42	0.018	1904.4887	12.89	0.018			
1868.5527	12.42	0.02	1904.5007	12.90	0.015			

fields than night-sky exposures, since they have an appreciably different spectrum; as a result, variations of the spectral sensitivity over the CCD field cannot be completely corrected.

In order to achieve maximum accuracy, we abandoned aperture photometry in favor of convolving a noisy image of the target with the response function. This approach makes it possible not only to achieve maximum signal-to-noise ratios for point sources in ideal conditions [6], but also to substantially decrease errors due to natural factors or the equipment.

Based on the above considerations, we developed software designed to process any number of images in an automated mode. As a result, we obtained for each CCD frame a list of parameters for all the detected objects.

In order to construct a light curve, all the images obtained under a variety of conditions and using two telescopes must be calibrated. This is usually done using several standard stars in the field of S5 0716+71. We decided not to use this approach, since the stability of such standards is not sufficient [7]. Assuming that the various objects detected in the frame are not physically associated, their variability should not be correlated, we carried out relative calibration of the S5 0716+71 images using all the objects detected in the field. To this end, we used our code [8], which cross-identifies lists of objects for two frames and then calculates the average flux ratio for identified objects. Since each frame contains 40 to 80 objects, the most pessimistic error for this calibration should not exceed 0.01^m. The code selects an image with maximum signal-to-noise ratio and then compares it with the other images.

Only this selected image is tied to the field standards in an absolute sense. We used Standards 3, 4, 5, and 6 from the studies [4, 7, 9] in the BVR filters, and Standards 3 and 5 from [7, 9] in the I filter. This

Table 2. Standard 5: stellar magnitudes obtained from field calibration procedure (see description in the text)

Filter	m	σ	$\langle\sigma\rangle$
B	14.16	0.034	0.018
V	13.54	0.019	0.015
R	13.16	0.018	0.014
I	12.86	0.018	0.018

approach reduced the influence of brightness variability of the standard stars to the maximum extent.

3. PHOTOMETRIC RESULTS

Table 1 presents data for S5 0716+71 in the four filters. Each line contains the Julian date of the observations together with the corresponding magnitude and its error.

Since the accuracy presented in Table 1 is a calculated parameter and thus depends on both the image quality and the reduction technique, it is natural to ask how realistic the values of this parameter are. The relative accuracy of the brightness determinations can be estimated independently from the rms deviation of the light curve of a stable object in the same frames as the studied object. We chose Standard 5, which is stable and close to 0716+71 in brightness, as such a stable object.

Table 2 presents our calibrations for Standard 5 in the four filters, which are consistent with published values for this star. Table 2 contains the mean magnitude, $m = \dfrac{\sum\limits_{i=1}^{n} m_i}{n}$; the rms deviation of the light curve, $\sigma = \sqrt{\dfrac{\sum\limits_{i=1}^{n} (m_i - m)^2}{n-1}}$; and the mean error of a single measurement, $\langle\sigma\rangle = \dfrac{\sum\limits_{i=1}^{n} \sigma_i}{n}$, where σ_i is the calculated error m_i, and n is the number of measurements over the total observing period.

We can see from Table 2 that σ exceeds $\langle\sigma\rangle$, particularly in B. This can be explained in two ways: either we have overestimated the accuracy, or Standard 5 displays weak variability.

Let us now consider Table 3, which presents the rms deviations for the differences between the light curves for Standard 5 in pairs of bands and the mean errors of these differences. It turned out

Table 3. Standard 5: differences in light curves and their errors

$m_1 - m_2$	$\langle m_1 - m_2\rangle$	σ_S	σ_{m1-m2}	$\langle\sigma_{12}\rangle$
$m_B - m_V$	0.615	0.039	0.024	0.023
$m_V - m_R$	0.379	0.026	0.016	0.021
$m_R - m_I$	0.304	0.025	0.016	0.024

that $\sigma_S = \sqrt{\sigma_1^2 + \sigma_2^2} > \sigma_{m1-m2}$, where σ_1 and σ_2 are taken from Table 2 for the two filters.

This implies that the light curves for Standard 5 in different filters are correlated, which, in turn, indicates that Standard 5 displays a weak but real variable component. Here,

$$\langle m_1 - m_2\rangle = \frac{\sum\limits_{i=1}^{n} (m_{1i} - m_{2i})}{n},$$

$$\sigma_{m1-m2} = \sqrt{\frac{\sum\limits_{i=1}^{n} (m_{1i} - m_{2i} - \langle m_1 - m_2\rangle)^2}{n-1}},$$

$$\langle\sigma_{12}\rangle = \frac{\sum\limits_{i=1}^{n} \sqrt{(\sigma_{1i}^2 + \sigma_{2i}^2)}}{n},$$

where σ_{1i} and σ_{2i} are the errors in m_{1i} and m_{2i}, respectively. Note that, for Standard 5, $\sigma_{m1-m2} \leq \langle\sigma_{12}\rangle$, thus that we have not overestimated the accuracy of our measurements.

The reality of the very rapid variability of S5 0716+71 is demonstrated by several fragments of the light curve (Fig. 1). We can clearly see from Fig. 1a that events are synchronous in all four bands. Figure 1b presents a fragment of the V and R light curve constructed from the data in Table 1 (JD−2450000 > 1142.4) that continues the data of [10]. Our data show good consistency between the V and R light curves, even in terms of the minor details that might have been considered to be errors if these observations had been carried out in the same band. The same graph presents the R light curve of Standard 5.

How regularly does the object exhibit rapid variability and can this information be derived from our data? Let us assume that observations in different filters are independent. A cross correlation of the light curves in two filters can then be used to judge whether these curves contain a correlated component related to a common brightness variability. The cross-correlation function was averaged over all the nights with no fewer than five exposures in each of the two filters. To decrease edge effects, we subtracted a linear trend from each night's light curves. The

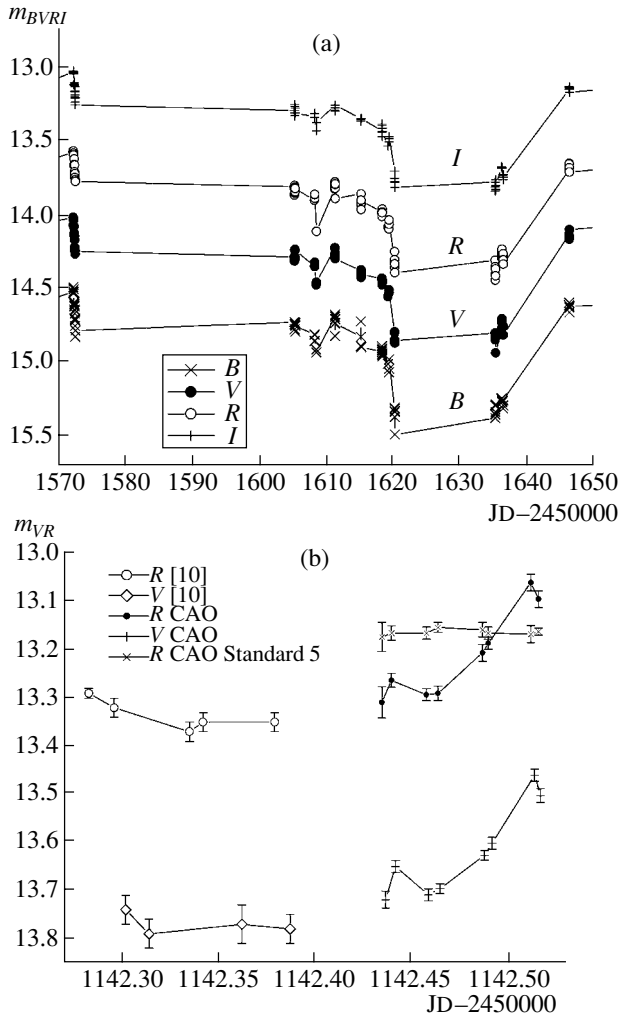

Fig. 1. Fragments of the S5 0716+71 light curve display variability in time scales of (a) days and (b) minutes. For JD−2450000 < 1142.4 presents the data of Qian et al. [10], and for JD−2450000 > 1142.4 data from Table 1 of the present study. Photometric measurements of Standard 5 in R are also presented.

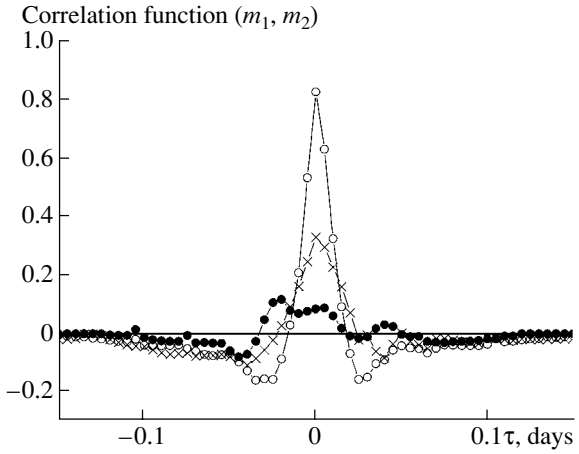

Fig. 2. Autocorrelation of the R light curve of S5 0716+71 (hollow circles), cross-correlation of the R and V light curves of S5 0716+71 (diagonal crosses), and cross-correlation of the R light curves of S5 0716+71 and Standard 5 (filled circles).

automated mode decreased the dispersion of intervals between the exposures during the night. The data for each night were interpolated in steps of 0.005 days (the interval between the times for the start of the exposures averaged over the entire observation period is 0.01 days).

Figure 2 presents the autocorrelation of the R light curve, the cross-correlation of the R and V light curves, and the cross-correlation of the R light curves for S5 0716+71 and Standard 5. This last curve shows that the identical processing used for the two objects did not introduce a similarity into the two light curves, even when the same images were used to derive the brightnesses of the two objects. The consistency between the width of the autocorrelation function, 0.014 days, and the average time between the exposures suggests that the variability spectrum continues towards high frequencies. The power spectrum derived from the cosine Fourier transform of the autocorrelation function, in the frequency interval $\nu = 3$–50 days^{-1} has the form ν^{-1}, and does not display any clearly distinguished harmonics. The cross-correlation function for the R and V light curves occupies an intermediate position between the autocorrelation function and the cross-correlation function for two independent processes. In contrast to the results of [11], the cross-correlation function does not display any significant shift between the V and R light curves. Reviewing the nights when this function was derived, we found time intervals when the correlation between the light curves was close to unity. Substantial brightness variations were usually observed in these intervals. There were also periods when the correlation was close to zero, when the brightness variability did not exceed the noise.

To estimate the behavior of the variability spectrum of S5 0716+71 over the broadest range of frequency as possible, we constructed a periodogram of the R light curves combined from four individual periodograms (Fig. 3a), following Terebizh [12]. The total observation time was divided into equal intervals, for each of which we derived a periodogram. These periodograms were then averaged over intervals of 0.3, 3, 30, and 300 days. The reason for this approach was that we wished to reach the highest frequencies as possible without a dramatic decrease in the accuracy. Since the time between exposures on some nights was appreciably shorter than the average (0.01 days), the spectrum was "extended" to a frequency of 100 days^{-1}.

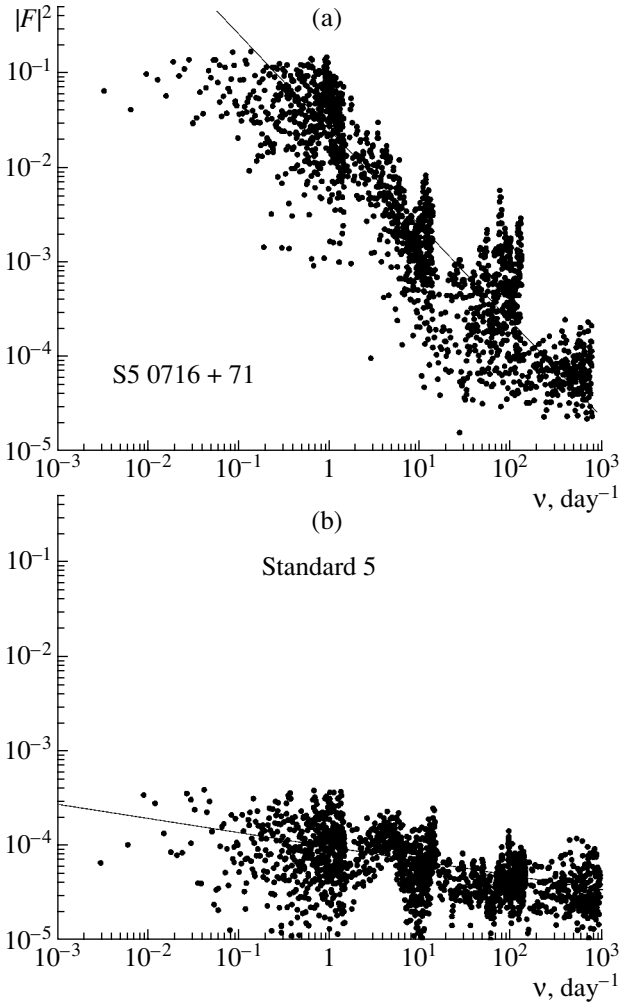

Fig. 3. Periodograms of R light curves of S5 0716+71 and Standard 5.

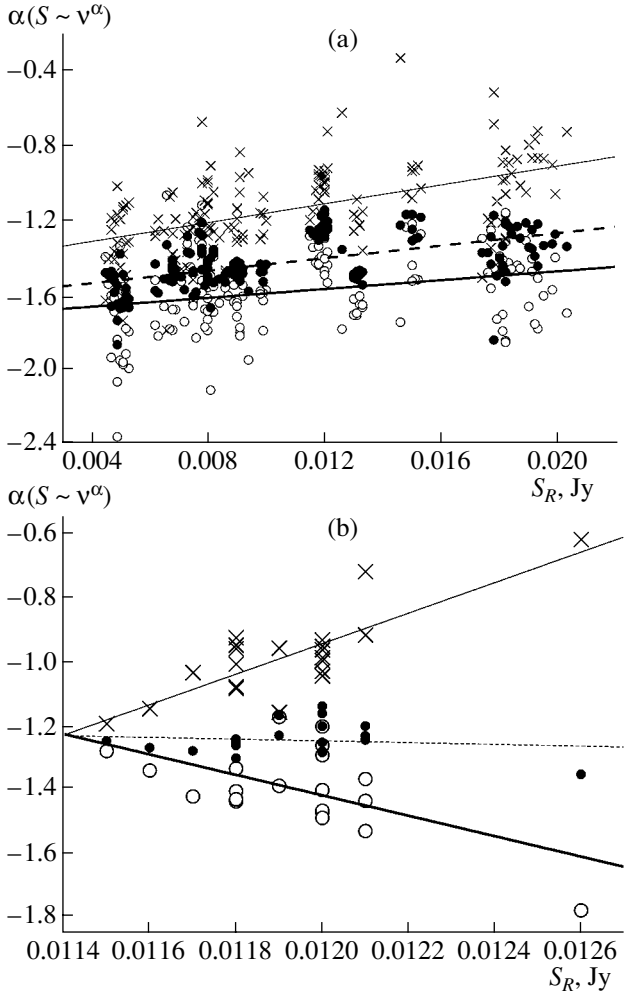

Fig. 4. The spectral index as a function of the flux for (a) the total observing time and (b) the night of December 25–26, 2000 in B (hollow circles), V (dark circles), and I (diagonal crosses).

For comparison, Fig. 3b presents the periodogram for the light curve of Standard 5 in the same intervals. The spectral slopes of the two objects are obviously different. The slope for the standard is $|F|^2 \propto \nu^{-0.15}$, while the slope for S5 0716+71 is $|F|^2 \propto \nu^{-1}$. This suggests that the variability of SF 0716+71 represents the classic flicker noise in the frequency interval 0.003–100 days^{-1}. The spectral slope of Standard 5 is apparently related to its weak variability. A periodogram for a model light curve generated for the set of observing times for a standard by adding a normally distributed error component to its average magnitude has zero slope over the entire frequency range.

We developed a code to "whiten" a periodogram in accordance with the recommendations given in [12], for use in distinguishing periodic components of the light curve. Applying this code to various time scales did not reveal any significant harmonic component in the light curve of S5 0716+71. Numerical experiments showed that a harmonic would have to have an amplitude of about 1^m to be detected against the background of the strong variability of the object.

Note the relation between the color and brightness of the object. Let us consider its spectrum in traditional radioastronomical "frequency–flux" coordinates. We selected time intervals when we had observations in all four filters. The average spectrum at frequencies 3.725×10^{14}–6.795×10^{14} Hz is described by the expression

$$\log S = 17.854 - 1.349 \log \nu, \qquad (1)$$

where S is the flux in Jansky, ν the frequency in Hz, and -1.349 is the mean spectral index. At a minimum brightness (March 16, 2000), the spectral index was $\alpha = -1.59$, while $\alpha = -1.13$ at a maximum brightness (December 20, 2000).

The average dependences between the spectral index and the flux at the edges (B, I) and in the

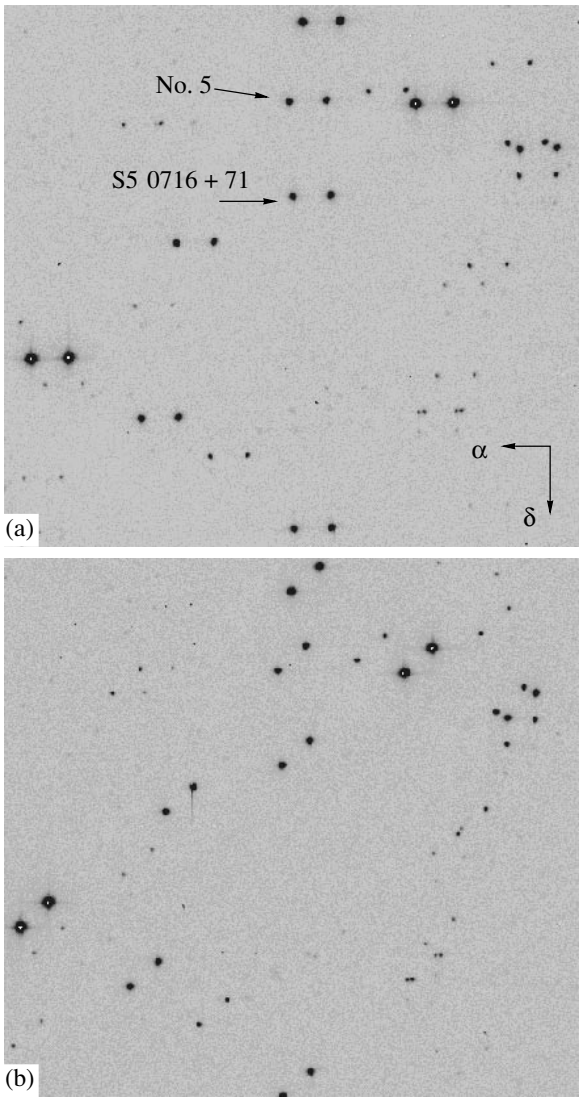

Fig. 5. Two exposures of the S5 0716+71 field obtained with a Zeiss-600 telescope in the V filter through the Savar plate with position angle 0° (left) and 45° (right).

center (V) of the optical wavelength interval covered is (Fig. 4a):

$$\bar{\alpha}_B = -1.7 + 11.9S \qquad \sigma = 0.22, \qquad (2)$$
$$\bar{\alpha}_V = -1.6 + 16.8S \qquad \sigma = 0.12,$$
$$\bar{\alpha}_I = -1.41 + 25.4S \qquad \sigma = 0.19.$$

Here, S is the mean flux in the frequency range ν_B–ν_I, and σ is the rms deviation of the spectral index from the average dependence. Then

$$\bar{\alpha}_B < \bar{\alpha}_V < \bar{\alpha}_I. \qquad (3)$$

It follows from these relations that an increase of the flux results in the flattening of the optical spectrum; i.e., the object becomes bluer. Relation (3) is obeyed in the total range of flux from 4–19 mJy.

The spectrum is, thus, convex. We note that the rms deviation of the spectral index substantially exceeds the scatter specified by the photometric errors (0.04–0.1) in all frequency ranges.

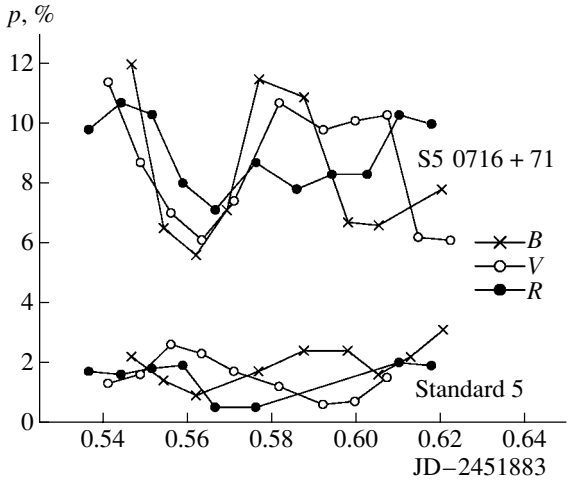

Fig. 6. Linear polarizations of S5 0716+71 and Standard 5 in BVR on April 12–13, 2000.

Let us consider the behavior of the spectral index for December 25–26, 2000 (Fig. 4b). During six hours of observations, 21 exposures were made in each filter. While the spectral index displays similar values $\alpha \sim -1.25$ at the minimum flux in all the bands, as the flux increases, the spectral indices at the edges of the frequency range deviate from this value in opposite directions. The rms deviations of the spectral indices relative to the average lines in B, V, and I are 0.1, 0.048, and 0.076, respectively, which are consistent with the photometric errors. Therefore, relation (2) is superimposed with rapid variability of the spectral index: an increase in flux is accompanied by an increase in negative curvature of the spectrum. At the same time, relation (3) is preserved. In this way, a flare occurs.

There naturally arise worries that we might observe the same pattern in the case of false fluctuations of the V and R brightness due to technical or computational errors. As a check, we repeated the above analysis using the data for Standard 5, but no significant spectral fluctuations were visible.

4. POLARIZATION: OBSERVATIONS AND REDUCTION

The linear polarization of the object was measured using a Savar plate, a polarizer made of two feldspar crystals with diameters of 30 mm and thicknesses of 7 mm, mounted on the rotating platform of the photometer guide in front of the CCD camera. When it passes through the polarizer, the object's image is split into two components separated by 1.1 mm. The linear polarization vectors of these components

Table 4. Linear polarization of the standard star HD 251204 at various epochs compared with our measurements

Epoch	*B*		*V*		*R*		Reference
	p, %	PA, deg	*p*, %	PA, deg	*p*, %	PA, deg	
Until 1989	–	–	4.04	147	–	–	[13]
Feb. 2, 1992	4.46	154.8	4.72	153.3	4.8	153	[14]
April 12, 2000	**3.5**	**141**	**5.35**	**154.5**	**3.41**	**158**	Our data
June 2, 2002	11.3	151.3	5.94	150.3	5.33	153.7	[14]

are orthogonal to each other, and make angles of 45° and 135° with a straight line connecting the components.

The polarizer parameters were calculated by I.D. Naĭdenov and manufactured in the optical workshop of SAO. Observations with a polarizer oriented in two different position angles are required to determine the linear polarization of the observed source. Rotation through an angle close to 45° was achieved by rotating the guide platform. Figure 5 presents the S5 0716+71 field observed with a Zeiss-600 telescope and polarizer.

The degree and position angle of the polarization were determined from the expressions

$$p = \frac{r_1 - 1}{(r_1 + 1)\cos\left(2\left(\varphi_1 - \phi\right)\right)}, \qquad (4)$$

$$\tan\left(2\left(\varphi_1 - \phi\right)\right) = \cot\left(2\left(\varphi_1 - \varphi_2\right)\right) - \frac{\left(r_2 - 1\right)\left(r_1 + 1\right)}{\left(r_2 + 1\right)\left(r_1 - 1\right)\sin\left(2\left(\varphi_1 - \varphi_2\right)\right)}.$$

Here, p is the linear polarization, r_1 the flux ratio of the components for polarizer position angle φ_1, r_2 the component flux ratio for polarizer position angle φ_2, and ϕ the position angle of the linear polarization.

The first stage of image processing is the same as in the photometric mode. The code then automatically selects from the obtained list of objects the pairs of components corresponding to each object in the field (we call them arbitrarily A and B) and forms two groups with the same number of A and B components. A weighted-average response function is constructed for each group, which is used to calculate the parameters of the objects in that group. Individual processing can be used to take into account the differences between the A and B images of the objects due to the small chromaticity of the polarizer (which can be seen from a careful inspection of Fig. 5). Further, the average orientation of the pairs, the average distance between the components, and the average component of flux ratio are calculated.

It is known from experience that most objects display very low polarization, substantially lower than our photometric accuracy, which specifies the scatter of the component flux ratios for the objects in the field. Therefore, this ratio differs from unity due to imperfections of the polarizer, spurious polarization created by the telescope optics, and the atmosphere. A robust estimate of this ratio yields a correction term that takes into account these factors.

5. RESULTS OF POLARIZATION MEASUREMENTS

Our observations were carried out on April 12–13, 2000, with a Zeiss-600 telescope. Figure 6 presents the polarization of S5 0716+71 as a function of time. The average polarization position angles in B, V, and R were $59° \pm 2.5°$, $64° \pm 1.2°$, and $64° \pm 1.5°$, respectively. The night average magnitude of an object in the same filters is 13.76, 13.38, and 12.91. No considerable relation between brightness and polarization oscillations is seen. The same plot for the photometric Standard 5 yields an average polarization of 1.5% with a scatter of 0.65%. The same values can be obtained in a simple model: the linear polarization of the standard star is zero, and the measurements have a photometric error of 0.016^m.

The polarimetric standard star HD 251204 was observed on the same night. Table 4 summarizes the previously published data of [13, 14] along with our results. It is clear that the two data sets are consistent, particularly in the V band.

This suggests that Fig. 6 displays real variations of the linear polarization of S5 0716+71 in a time scale of 15–30 min. The graph is even suggestive of a correlation between the variations in the three filters (that can be seen by the eye). At the time of these observations, the average polarizations in BVR were 8.3, 8.5, and 9%, while the spreads in these values covered 6.4, 5.3, and 3.6%, respectively. The error in the polarization measurements estimated from the observations of Standard 5 in all filters is 0.65%.

Rapid variations of polarization of S5 0716+71 were previously mentioned in [15].

6. CONCLUSIONS

Our observations suggest that the enigmatic object S5 0716+71 displays variability of its brightness and linear polarization on a wide range of time scales down to 5–10 min. The object's spectral variability corresponds to the classic flicker noise. The total time of our observations was insufficient to detect any harmonic component of the brightness variations. The optical spectrum of S5 0716+71 in the interval I–B (3.725×10^{14}–6.795×10^{14} Hz) flattens as the brightness increases. During short flares, the curvature of the spectrum increased, and rapid fluctuations were superimposed with slow variations of the spectral index.

Like most researchers, we assume that the optical emission of S5 0716+714 is synchrotron radiation by relativistic electrons. However, an ideal model with a homogeneous particle flux is not able to explain rapid variability and its synchronicity over a broad range of wavelengths. We suggest that the flux is inhomogeneous, with the size of the inhomogeneities being substantially smaller than the radius of the jet. If we (bravely) estimate the size of the inhomogeneities from the formula of Slysh [16], assuming that the maximum of a flare lies in the optical, we obtain $\sim 10^{-10}$–10^{-11} arcsec. The radiation from an ensemble of compact inhomogeneities of this size that are in different stages of their evolution can then easily explain the observed pattern. We hope to consider this model further in our next study.

ACKNOWLEDGMENTS

The author thanks the researchers of the Special Astrophysical Observatory of the Russian Academy of Sciences V.V. Vlasyuk, V.P. Mikhaĭlov, and O.I. Spiridonova, who actively observed the object studied here.

REFERENCES

1. H. Kuhr, I. I. K. Pauliny-Toth, A. Witzel, and J. Schmidt, Astron. J. **86**, 854 (1981).
2. S. J. Wagner and A. Witzel, Annu. Rev. Astron. Astrophys. **33**, 163 (1995).
3. S. J. Wagner, A. Witzel, J. Heidt, et al., Astron. J. **111**, 6 (1996).
4. M. Villata, C. M. Raiteri, L. Lanteri, et al., Astron. Astrophys., Suppl. Ser. **130**, 305 (1998).
5. V. R. Amirkhanyan, N. A. Vikul'ev, V. V. Vlasyuk, and D. A. Stepanian, Bull. Spec. Astrophys. Obs. **50**, 142 (2000).
6. N. S. Shestov, *Extraction of Optical Signals against a Background of Random Noise* (Sov. Radio, Moscow, 1967) [in Russian].
7. R. Sagar, Gopal-Krishna, V. Mohan, et al., Astron. Astrophys., Suppl. Ser. **134**, 453 (1999).
8. V. R. Amirkhanyan, Preprint No. 77, SAO (Spec. Astrophys. Obs., Crimea, 1991), p. 3.
9. G. Ghisellini, M. Villata, C. M. Raiteri, et al., Astron. Astrophys. **327**, 61 (1997).
10. B. Qian, J. Tao, and J. Fan, Astrophys. J. **123**, 678 (2002).
11. M. Villata, J. R. Mattox, E. Massaro, et al., Astron. Astrophys. **363**, 108 (2000).
12. V. Yu. Terebizh, *Time Series Analysis in Astrophysics* (Nauka, Moscow, 1992) [in Russian].
13. D. A. Turnshek, R. C. Bohlin, R. L. Williamson, et al., Astron. J. **99**, 1243 (1990).
14. http://www.sal.wisc.edu/HPOL/tgts/HD251204.html.
15. C. D. Impey, V. Bychkov, S. Tapia, et al., Astron. J. **119**, 1542 (2000).
16. V. I. Slish, Nature **200**, 56 (1963).

Translated by K. Maslennikov